www.czasopisma.pan.pl PAN POLSKA AKADEMIA NAUK www.journals.pan.pl

Archives of Acoustics Vol. 48, No. 3, pp. 359–372 (2023), doi: 10.24425/aoa.2023.145240

Research Paper

Study on Noise Attenuation Characteristics of Hydrofoil with Specific Cavitation Number

He XIAOHUI(1)*, Liu ZHONGLE(2), Yang CHAO(1), Yuan ZHIYONG(2)

(1) *Jiangnan Industry Group Co., Ltd.*
Wuyi Village, China

(2) *Naval University of Engineering*
Wuhan, China

*Corresponding Author e-mail: xiaohui.he16@gmail.com

(*received September 23, 2022; accepted January 26, 2023*)

In this study, the modified Sauer cavitation model and Kirchhoff-Ffowcs Williams and Hawkings (K-FWH) acoustic model were adopted to numerically simulate the unsteady cavitation flow field and the noise of a three-dimensional NACA66 hydrofoil at a constant cavitation number. The aim of the study is to conduct and analyze the noise performance of a hydrofoil and also determine the characteristics of the sound pressure spectrum, sound power spectrum, and noise changes at different monitoring points. The noise change, sound pressure spectrum, and power spectrum characteristics were estimated at different monitoring points, such as the suction side, pressure side, and tail of the hydrofoil. The noise characteristics and change law of the NACA66 hydrofoil under a constant cavitation number are presented. The results show that hydrofoil cavitation takes on a certain degree of pulsation and periodicity. Under the condition of a constant cavitation number, as the attack angle increases, the cavitation area of the hydrofoil becomes longer and thicker, and the initial position of cavitation moves forward. When the inflow velocity increases, the cavitation noise and the cavitation area change more drastically and have a superposition tendency toward the downstream. The novelty is that the study presents important calculations and analyses regarding the noise performance of a hydrofoil, characteristics of the sound pressure spectrum, and sound power spectrum and noise changes at different monitoring points. The article may be useful for specialists in the field of engineering and physics.

Keywords: sound pressure spectrum; noise; sound power spectrum; numerical prediction.

1. Introduction

Cavitation, the formation of bubbles in a liquid, is a phenomenon that generally occurs at the interface between a fluid and a solid with relative motion (Cao *et al.*, 2014). In other words, when the local pressure in the flow field drops to the saturated vapor pressure at its proper temperature, the liquid medium will explosively vaporize and form bubbles. When cavitation reaches a certain threshold, it will be accompanied by the burst and detachment of bubble groups, which causes strong noise, vibration and cavitation erosion (Sultanov *et al.*, 2020). The spatial differences of the closing emerge throughout the cavity's development, and under specific circumstances, the pocket becomes unstable and violently implodes. The volume of the vapor cavity oscillates between a minimum and a maximum during this operating regime. The destabilizing process results in the emission of biphasic and vortex structures known as cavitation clouds, which are highly erosive and known to produce large overpressures.

Cavitation flow encompasses almost all complex flow phenomena: turbulence, multiphase flow, phase transition, compressible, and unsteady characteristics, etc., (Huang *et al.*, 2018; Prokopov *et al.*, 1993). Cavitation can be divided into different forms: primary cavitation, sheet cavitation, cavitation cloud, eddy cavitation, and super-cavitation (Wang *et al.*, 2001). Cavitation often has adverse effects on underwater and water conservancy equipment, for example, by reducing thrust efficiency, severely corroding the structure of equipment, and affecting normal performance

(Chang, 2011; Shin *et al.*, 2021). On the other hand, scholars and engineers have also explored the potential benefits of cavitation. For example, it is used for sterilizing and crushing stones in the medical field, industrial sewage treatment, oil exploitation, underwater cutting, shock absorption, noise reduction for underwater weapons, etc.

Many scholars have conducted extensive theoretical and experimental research on hydrofoils and acoustic radiation. From a theoretical perspective, Euler proposed the cavitation phenomenon for the first time in 1753. In 1839, Reynolds and Besant (Li, Shi, 1997) studied cavitation in the laboratory. Lord Rayleigh (1917) formulated the mathematical equation of cavitation bubbles in an incompressible fluid, and Plesset (1949) made a correction to the theory of Rayleigh. Noltingk, Neppiras (1950) and Neppiras, Noltingk (1951) added an additional pressure correction to the surface tension in the Rayleigh model, and in 1952, Poritsky added a liquid viscosity correction (Korzhyk *et al.,* 2017). Since then, many scholars have continuously developed this theory.

An important work is presented in (Wang *et al.*, 2021). The research examines the effect of water injection on broadband noise and hydrodynamic performance for NACA66 (MOD) hydrofoils under cloud cavitation conditions. The influence of water injection on the hydrodynamic performance and noise sources for a NACA66 (MOD) hydrofoil under cloud cavitation is computed in this work ($\sigma = 0.83$, $\mathrm{Re} = 5.1\times10^5$). The results of the analysis show that the water injection may effectively stop the growth of cloud cavitation and significantly reduce the severe pressure fluctuation. As a result, the flow field's dipole/quadrupole noise can be reduced. Kubota *et al.* (1992) proposed a cavitation model based on the transport equation on the basis of the Rayleigh–Plesset equation. Based on the Rayleigh–Plesset equation, Zwart (2004), Schnerr, Sauer (2001), and Singhal *et al.* (2002) established their respective cavitation transport equations representing the relationship between mass transport and pressure change. Kieldsen *et al.* (2000) conducted experimental research on a NACA0015 hydrofoil. From an experimental perspective, Leroux *et al.* (2003; 2004) carried out a study on the fracture and detachment phenomenon of cavitation generated by the unsteady cavitation of a single NACA66 hydrofoil. Fuji *et al.* (2007) studied the influence of the geometric shapes of hydrofoils on cavitation dynamics and summarized NACA0015 hydrofoil decrease in different water holes. Through FFT analysis, the influence of instability on cavitation dynamics was obtained. Hong *et al.* (2017) studied the Clark-Y hydrofoil characteristics with different cavitation numbers.

Wang *et al.* (2009) and Zhang *et al.* (2009) performed a time-frequency analysis on the unsteady dynamic characteristics of the cavitation around the hydrofoil. Ducoin *et al.* (2009; 2012), Wu *et al.* (2005), Wang, Ostoja-Starzewski (2007), Ji *et al.* (2010), and others studied fluid-solid coupling and the cavitation of two-dimensional and three-dimensional hydrofoils by combining numerical simulation and experiments. Fan (2015) performed research on the vibration and acoustic radiation of a hydrofoil. The purpose of the article is to conduct and analyze numerically the unsteady cavitation flow field and the noise of a three-dimensional NACA66 hydrofoil under a constant cavitation number.

2. Materials and methods

2.1. Mathematical, noise, and cavitation models

In the calculation process, the homogeneous equilibrium flow model is adopted. Assuming that there is no velocity slip between the gas and liquid, the mass conservation equation, the momentum equation, and the density equation of a three-phase mixture are, respectively:

Mass equation:

$$\frac{\partial \rho_m}{\partial t} + \nabla \cdot (\rho_m u) = 0. \tag{1}$$

Momentum equation:

$$\frac{\partial \rho_m u}{\partial t} + \nabla \cdot (\rho_m u u) = -\nabla p + \nabla \cdot \tau + S_M, \tag{2}$$

where $\tau = \mu\left(\nabla u + (\nabla u)^T - \frac{2}{3}\delta \nabla \cdot u\right)$.

The density of the mixture is defined by the equation:

$$\rho_m = a_l \rho_l + a_v \rho_v + a_g \rho_g, \tag{3}$$

where a_l, a_v, and a_g represent the volume fraction of gas in the liquid phase, vapor phase and non-condensation state, respectively, and ρ_l, ρ_v, and ρ_g refer to the densities of gas in these three states, respectively.

Mass fraction:

$$y_i = \frac{a_i \rho_i}{\rho_m}. \tag{4}$$

In the numerical calculation, the turbulence motions are roughly divided into three types: firstly, direct simulation (DNS), secondly, large eddy simulation (LES), and thirdly, Reynolds-averaging averaging simulation.

In this study, the large eddy simulation model (LES model) was adopted to solve the transient Navier–Stokes equation, which can directly simulate large eddies in turbulence, but not small eddies. As a result, a similar model was established to simulate the influence of small eddies on large ones. That is, the Navier–Stokes equation is filtered in the wavenumber space or physical space. The filtering process removes small eddies, the width of which is less than the filtering width

or the given physical width, in order to obtain the control equation of large eddies (Alkishriwi *et al.*, 2008):

$$\overline{\Phi}(x) = \int_D \Phi(x')G(x;x') \lim_{x\to\infty} \mathrm{d}x', \tag{5}$$

where D is the fluid domain, G is the filter function that determines the scale of the resolved eddies, and Φ is defined by $\Phi' = \Phi - \overline{\Phi}$ and $\overline{\Phi'} \neq 0$.

The discretization of the spatial domain into finite control volumes implicitly provides the filtering operation:

$$\overline{\Phi}(x) = \frac{1}{V}\int_V \Phi(x')\,\mathrm{d}x', \quad x' \in V, \tag{6}$$

where V is the control volume. The filter function $G(x;x')$ implied here is then:

$$G(x;x') = \begin{cases} 1/V, & x' \in V, \\ 0, & \text{otherwise.} \end{cases} \tag{7}$$

Filtering the Navier–Stokes equations leads to additional unknown quantities. The filtered momentum equation can be written in the following way:

$$\frac{\partial}{\partial t}\left(\overline{\rho}\,\overline{U}_i\right) + \frac{\partial}{\partial x_j}\left(\overline{\rho}\,\overline{U}_i\overline{U}_j\right) = -\frac{\partial \overline{p}}{\partial x_i} + \frac{\partial}{\partial x_j}\left[\mu\left(\frac{\partial \overline{U}_i}{\partial x_j} + \frac{\partial \overline{U}_j}{\partial x_i}\right)\right] + \frac{\partial \tau_{ij}}{\partial x_j}, \tag{8}$$

where τ_{ij} denotes the subgrid-scale stress:

$$\tau_{ij} = \rho\overline{U}_i\,\overline{U}_j - \overline{\rho}\,\overline{U}_i\,\overline{U}_j. \tag{9}$$

Flow-induced noise is generated by the disturbance propagation in the flow process. The disturbance propagation generates pressure fluctuations and propagates outward as a sound source. The boundary layer of the hydrofoil and the detachment of eddies radiate high-frequency noise, which is equivalent to the quadrupole source. The non-uniform flow field around the hydrofoil and the unsteady pulsation force on the hydrofoil surface induced by the pulsation turbulence field radiate low-frequency noise, which is equivalent to the dipole source, and the noise caused by the burst of bubbles is equivalent to the monopole.

The right side of the equation hereinafter refers to two surface source items (monopole and dipole) and one volume source item (quadrupole). The formula consists of a volume integral polynomial and a surface integral polynomial; the surface integral describes the contribution of the monopole source, dipole source, and part of the quadrupole source to the noise, while the volume integral defines the quadrupole contribution outside the control surface. If the quadrupole item is ignored, the equation of the pressure field is defined as:

$$p'(x,t) = p'_T(x,t) + p'_L(x,t). \tag{10}$$

The corresponding monopole, $p'_T(x,t)$, is the sound pressure due to the thickness. The corresponding dipole, $p'_L(x,t)$, defines the sound pressure due to the load. The formula is shown in Eqs. (11) and (12):

$$4\pi p'_T(x,t) = \int_{f=0}\left[\frac{\rho_0\dot{v}_n}{r(1-M_r)^2}\right]\mathrm{d}S + \int_{f=0}\left[\frac{\rho_0 v_n\left[r\dot{M}_r\widehat{r}_i + c_0(M_r - M^2)\right]}{r^2(1-M_r)^3}\right]\mathrm{d}S, \tag{11}$$

$$4\pi p'_L(x,t) = \frac{1}{c_0}\int_{f=0}\left[\frac{l_i\widehat{r}_i}{r(1-M_r)^2}\right]\mathrm{d}S + \int_{f=0}\left[\frac{l_r - l_i M_i}{r(1-M_r)^2}\right]\mathrm{d}S + \frac{1}{c_0}\int_{f=0}\left[\frac{l_r\left[r\dot{M}_r\widehat{r}_i + c_0(M_r - M^2)\right]}{r^2(1-M_r)^3}\right]\mathrm{d}S, \tag{12}$$

where M refers to the Mach number, M_r represents the radial Mach number, and l_i is the local force on the unit area at the direction of i, which can also be defined by Eqs. (13) and (14) (Beljatynskij *et al.*, 2010; Curle, 1955; Nurtas *et al.*, 2020; Prentkovskis *et al.*, 2012; Su *et al.*, 2013; Yang *et al.*, 2014):

$$p'_T(x,t) = \int_{-T}^{T}\int_{A(\tau)} \rho v_n \frac{DG}{D\tau}\,\mathrm{d}A(y)\,\mathrm{d}\tau, \tag{13}$$

$$p'_L(x,t) = \int_{-T}^{T}\int_{A(\tau)} F_i \frac{DG}{D\tau}\,\mathrm{d}A(y)\,\mathrm{d}\tau. \tag{14}$$

A cavitation model mathematically describes the mutual transformation between water and vapor, which can be characterized by the modified Sauer cavitation model proposed by Yang *et al.* (2011; 2012):

$$\dot{m}^+ = \frac{C_{\mathrm{prod}}3a_g(1-a_v)\rho_v}{R_B}\sqrt{\frac{2}{3}\frac{|P_v - P|}{\rho_l}}\,\mathrm{sign}\,(P_v - P), \tag{15}$$

$$\dot{m}^- = C_{\mathrm{dest}}\frac{3a_v\rho_v}{R_B}\sqrt{\frac{2}{3}\frac{|P_v - P|}{\rho_l}}\,\mathrm{sign}\,(P_v - P), \tag{16}$$

where $\dot{m}^+$ and $\dot{m}^-$ represent evaporation and condensation of vapor, the mass fraction is $a_g = 7.8\times10^{-4}$, the volume fraction is $a_v = 1\times10^{-6}$, R_B is the initial value of the bubble radius, $R_B = 1.0\times10^{-6}m$, the evaporation coefficient is $C_{\mathrm{prod}} = 50$, the condensation coefficient is $C_{\mathrm{dest}} = 0.01$, and $P_v = P_{\mathrm{sat}} + 0.5P_{\mathrm{turb}}$, and $P_{\mathrm{turb}} = 2\rho k/3$.

2.2. Divisions of geometric models and computational domain

A NACA66 hydrofoil was used as the research geometric model. The geometric parameters were obtained from Plesset (1949), and the unsteady calculation was conducted in order to study the acoustic radiation law of the hydrofoil with different inflow velocities and different attack angles for a specific cavitation number (Al-Obaidi, 2019, 2020; Al-Obaidi, Mishra, 2020):

$$\text{cavitation number:} \quad \sigma_n = \frac{P - P_V}{\frac{1}{2}\rho V^2}, \tag{17}$$

$$\text{pressure coefficient:} \quad C_p = \frac{P - P_V}{\frac{1}{2}\rho V^2}, \tag{18}$$

$$\text{Strouhal number:} \quad \text{St} = \frac{fc}{V}, \tag{19}$$

$$\text{Reynolds number:} \quad \text{Re} = \frac{Vc}{v}, \tag{20}$$

where P is the environmental pressure, P_V is the saturated vapor pressure, V is the inflow velocity, f is the falling-off period of the cavity, c is the chord length of the hydrofoil, and v is the viscosity coefficient.

The computational domain setting is shown in Figs. 1 and 2 (geometric model establishment and grid division).

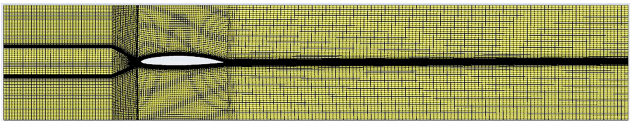

Fig. 1. The whole computational domain.

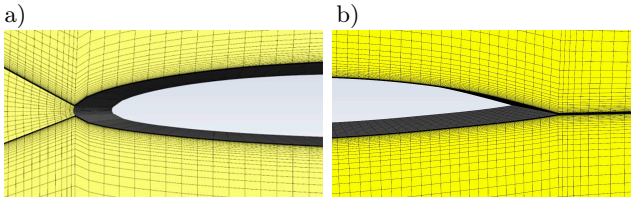

Fig. 2. Close-up view of mesh near the leading edge and the trailing edge of the hydrofoil: a) leading edge near the foil (LE); b) trailing edge near the foil (TE).

To reduce computational resources, the distance between the leading edge of the foil and the incoming flow is set to 2 c, the distance between the leading edge of the foil and the outlet of pressure is 6 c, the foil span is 0.3 c, and the height of the three-dimensional computational domain is 1.28 c. Cavitation number σ_n: 1.25; total working conditions of attack angles: 11, namely, 0°, ±3°, ±6°, ±9°, ±12°, and ±15°; inflow velocity: 5.33 m/s, 10.288 m/s, and 20.577 m/s; environmental pressure: 21263.6 P_a, 71279.5 P_a, and 267697 P_a.

The coordinates of the noise monitoring points are set. There are 31 noise monitoring points in total, whose coordinates are shown in Table 1.

Table 1. Settings of monitoring points (Z–0).

Monitoring points	X [mm]	Y [mm]
R1	0	0
R2	12.1195	4.9922
R3	37.5488	7.6615
R4	48.601	7.8085
R5	68.403	6.5358
R6	81.82	4.413
R7	100	–0.1178
R8	100	50
R9	100	100
R10	150	0
R11	150	50
R12	150	100
R13	200	0
R14	200	50
R15	200	100
R16	300	0
R17	300	50
R18	300	100
R19	13.2317	–2.9933
R20	36.6214	–3.9267
R21	47.689	–3.9042
R22	73.21	–2.6703
R23	91.23	–1.2005
R24	100	–50
R25	100	0
R26	150	–50
R27	150	–100
R28	200	–50
R29	200	–100
R30	300	–50
R31	300	–100

3. Results and discussion

When the inflow velocity is 5.33 m/s and the cavitation number is 1.25 (σ_n = 1.25), the simulation result is in good agreement with the experimental result of Leroux *et al.* (2004). In addition, typically unstable cloud cavitation occurs, and it can be observed that a large number of vortexes detach from the surface of the foil (Leroux *et al.*, 2004). The surface load of the foil also changes, and the lift and drag coefficients undergo a certain periodic change. When the length of

the cavity is less than 0.5 c, the bubble groups fluctuate less on the surface of the foil: such cavitation is called quasi-stable cavitation. However, when the length of the cavity is greater than 0.5 c, the cavity structure becomes quite unstable, and the bubbles burst. Cavitation pressure pulsation and the length of the cavity change regularly from the top of the blades. When the length of the cavity L/C reaches the maximum value of 0.7~0.8, it is called unstable cavitation. After verifying that the simulation is correct, the cavitation number is fixed at σ_n = 1.25, and then the second working condition (inflow velocity of 10.288 m/s) and the third working condition (inflow velocity of 20.577 m/s) are selected.

Noise law of cavity in the unsteady growth process:
– working condition 1 – 5.33 m/s, Figs. 3–8;
– working condition 2 – 10.288 m/s, Figs. 9–14;
– working condition 3 – 20.577 m/s, Figs. 15–20.

Overall sound pressure level analysis:
– working condition 1 – 5.33 m/s, Figs. 21–22;
– working condition 2 – 10.288 m/s, Fig. 23;
– working condition 3 – 20.577 m/s, Fig. 24.

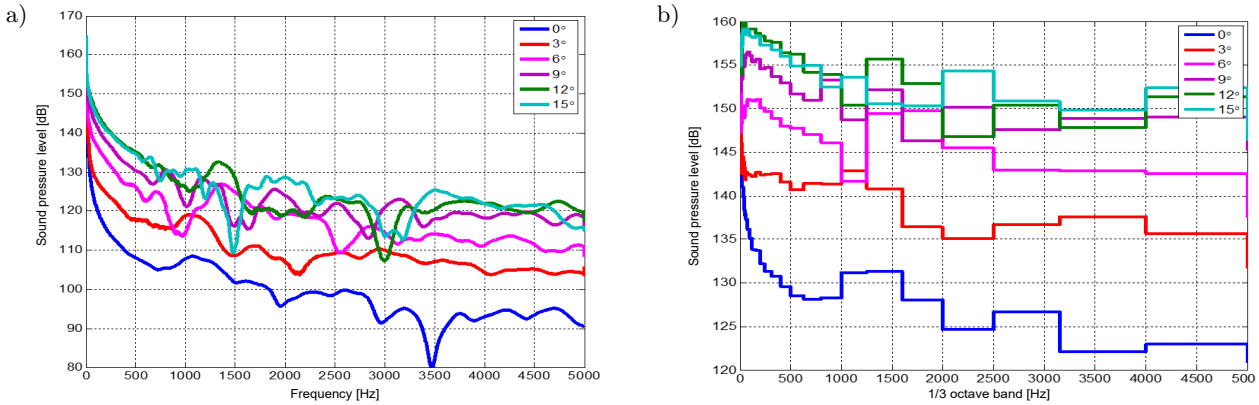

Fig. 3. Sound pressure frequency spectrum curves of R1 at 0°, 3°, 6°, 9°, 12°, 15° (cavitation number is fixed at σ_n = 1.25).

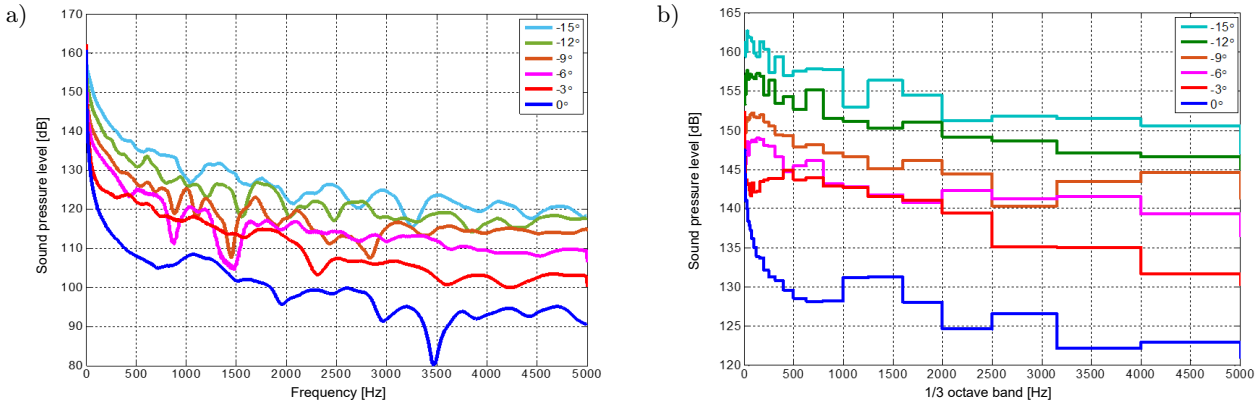

Fig. 4. Sound pressure frequency spectrum curves of R1 at 0°, –3°, –6°, –9°, –12°, –15°.

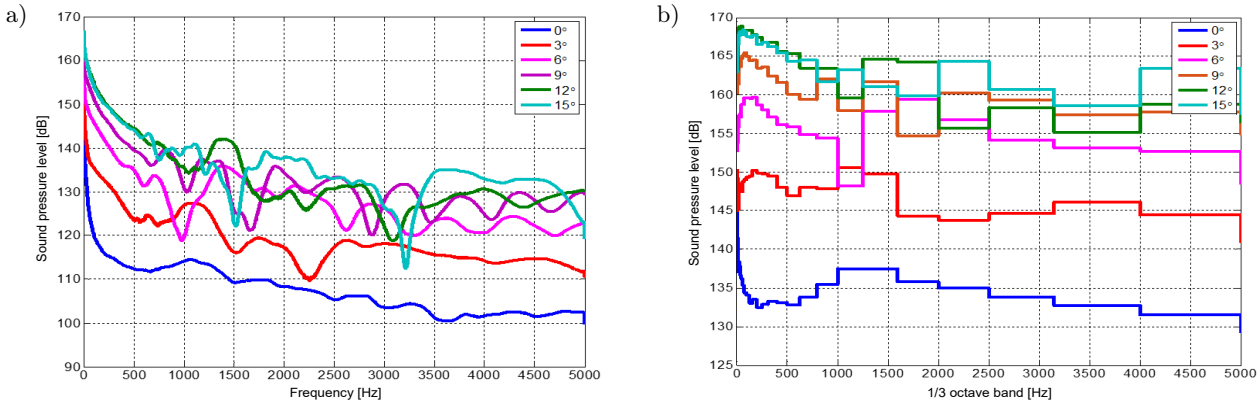

Fig. 5. Sound pressure frequency spectrum curves of R6 at 0°, 3°, 6°, 9°, 12°, 15°.

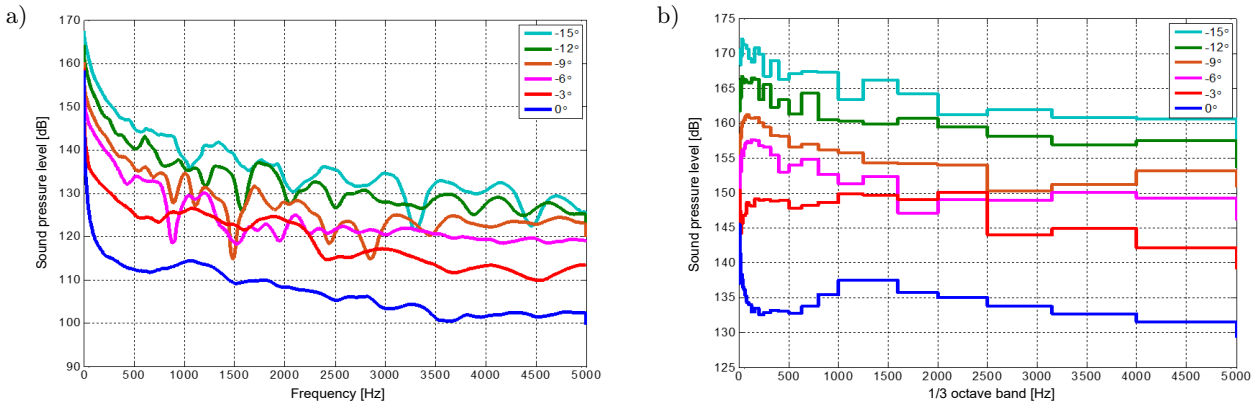

Fig. 6. Sound pressure frequency spectrum curves of R6 at 0°, –3°, –6°, –9°, –12°, –15°.

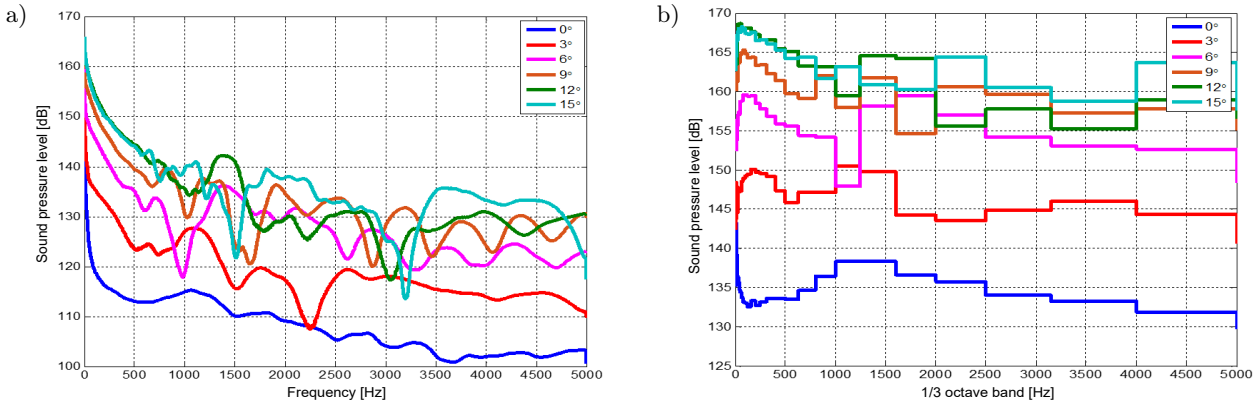

Fig. 7. Sound pressure frequency spectrum curves of R7 at 0°, 3°, 6°, 9°, 12°, 15°.

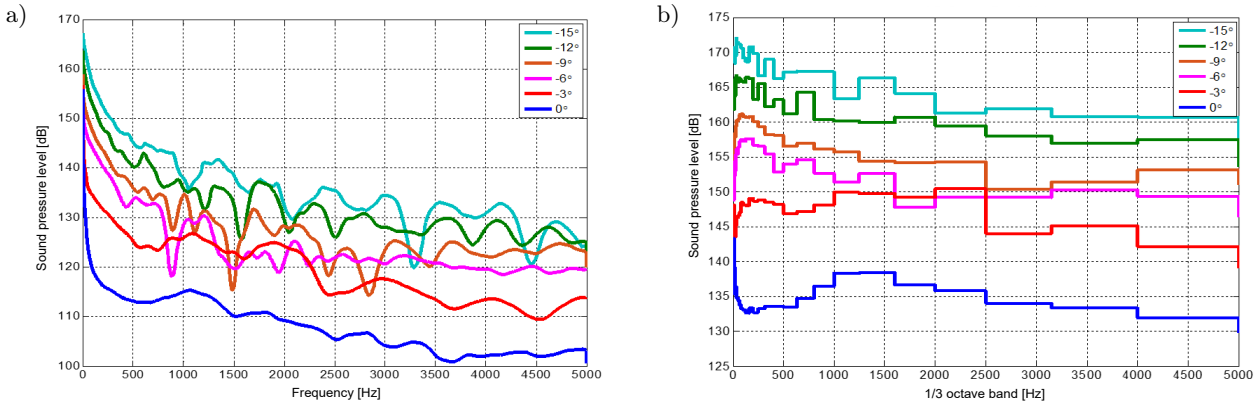

Fig. 8. Sound pressure frequency spectrum curves of R7 at 0°, –3°, –6°, –9°, –12°, –15°.

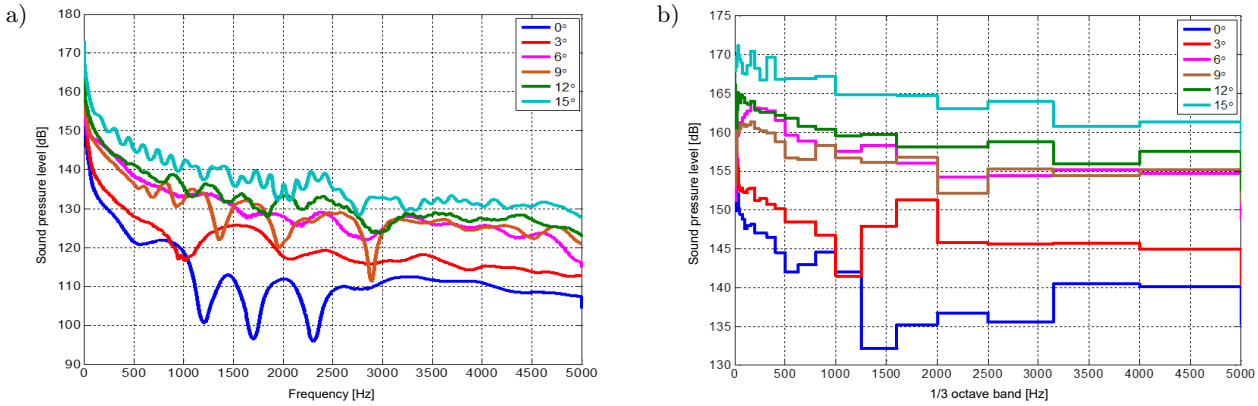

Fig. 9. Sound pressure frequency spectrum curves of R1 at 0°, 3°, 6°, 9°, 12°, 15°.

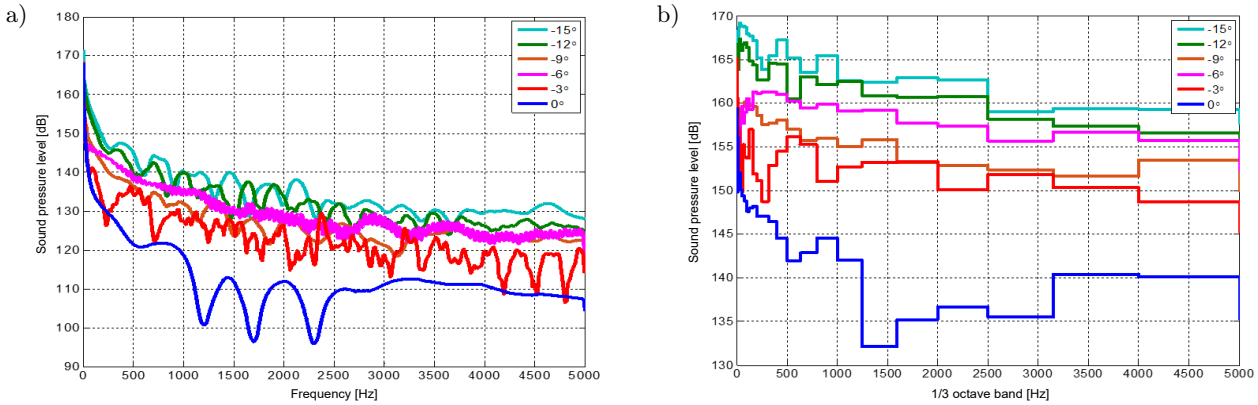

Fig. 10. Sound pressure frequency spectrum curves of R1 at 0°, –3°, –6°, –9°, –12°, –15°.

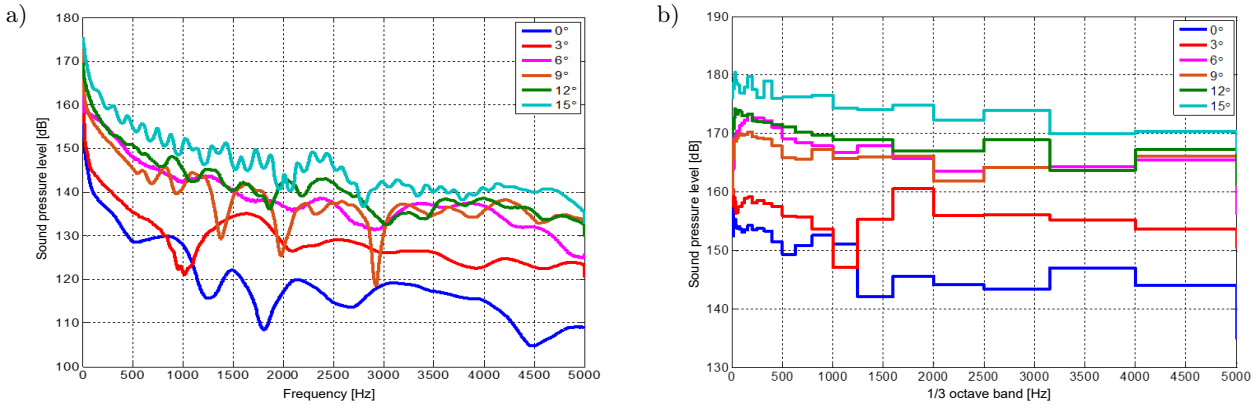

Fig. 11. Sound pressure frequency spectrum curves of R6 at 0°, 3°, 6°, 9°, 12°, 15°.

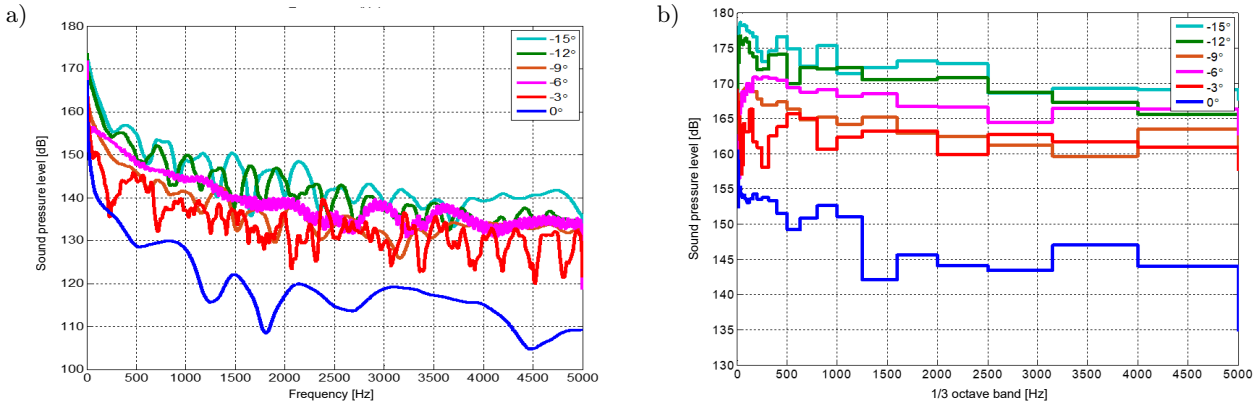

Fig. 12. Sound pressure frequency spectrum curves of R6 at 0°, –3°, –6°, –9°, –12°, –15°.

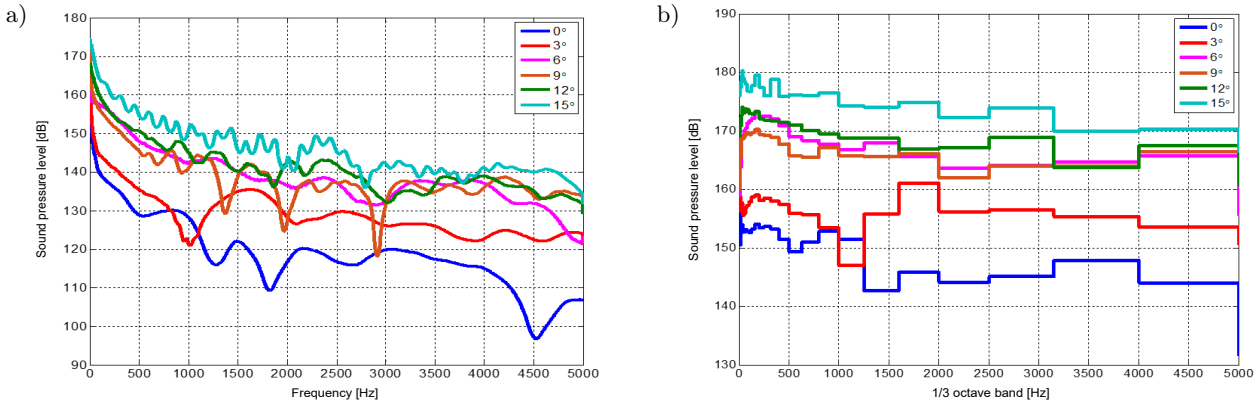

Fig. 13. Sound pressure frequency spectrum curves of R7 at 0°, 3°, 6°, 9°, 12°, 15°.

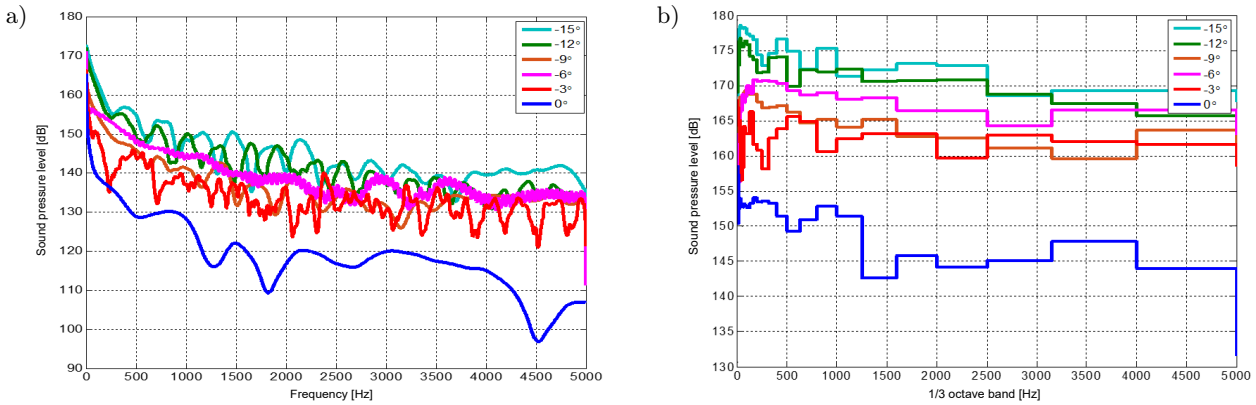

Fig. 14. Sound pressure frequency spectrum curves of R7 at 0°, –3°, –6°, –9°, –12°, –15°.

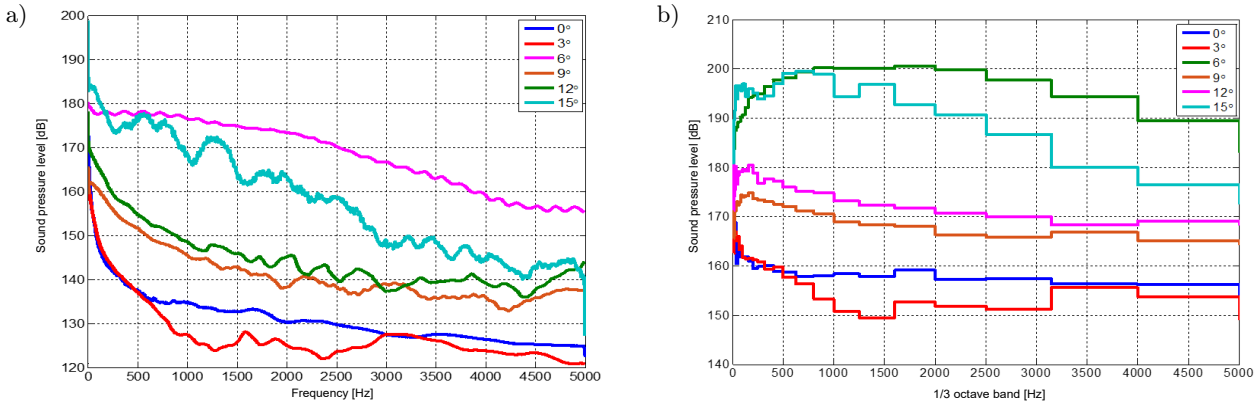

Fig. 15. Sound pressure frequency spectrum curves of R1 at 0°, 3°, 6°, 9°, 12°, 15°.

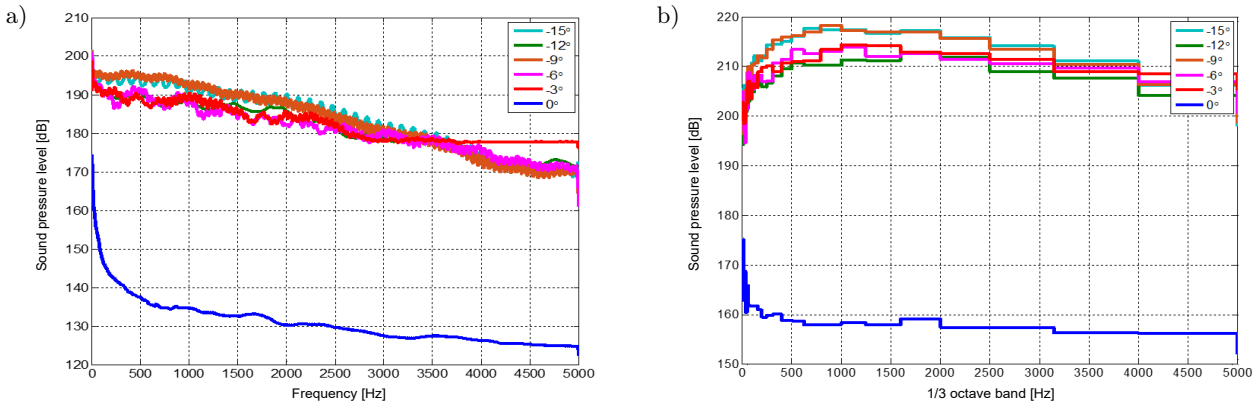

Fig. 16. Sound pressure frequency spectrum curves of R1 at 0°, –3°, –6°, –9°, –12°, –15°.

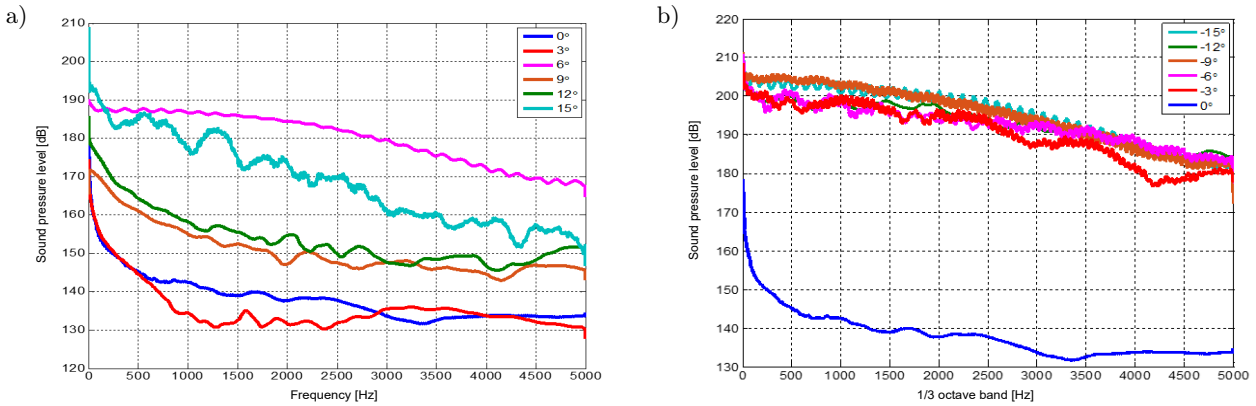

Fig. 17. Sound pressure frequency spectrum curves of R6 at 0°, 3°, 6°, 9°, 12°, 15°.

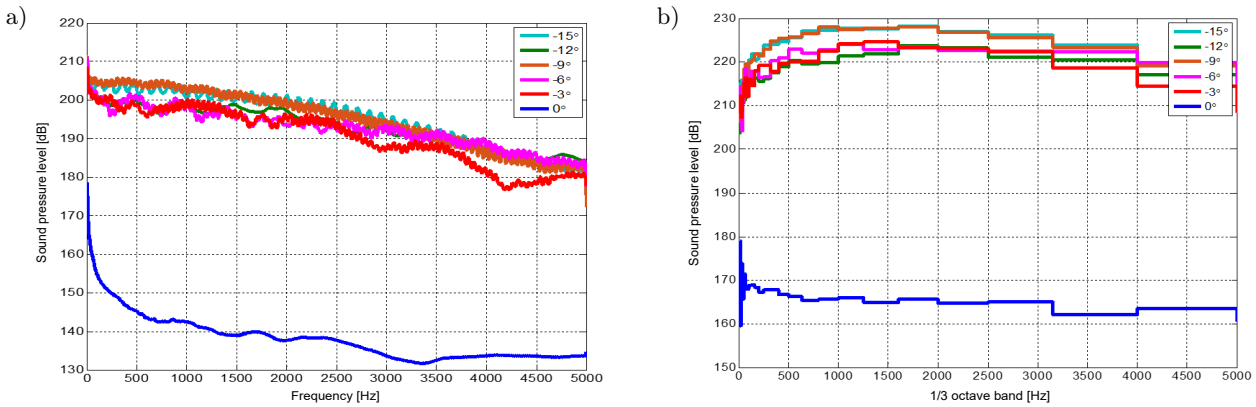

Fig. 18. Sound pressure frequency spectrum curves of R6 at 0°, −3°, −6°, −9°, −12°, −15°.

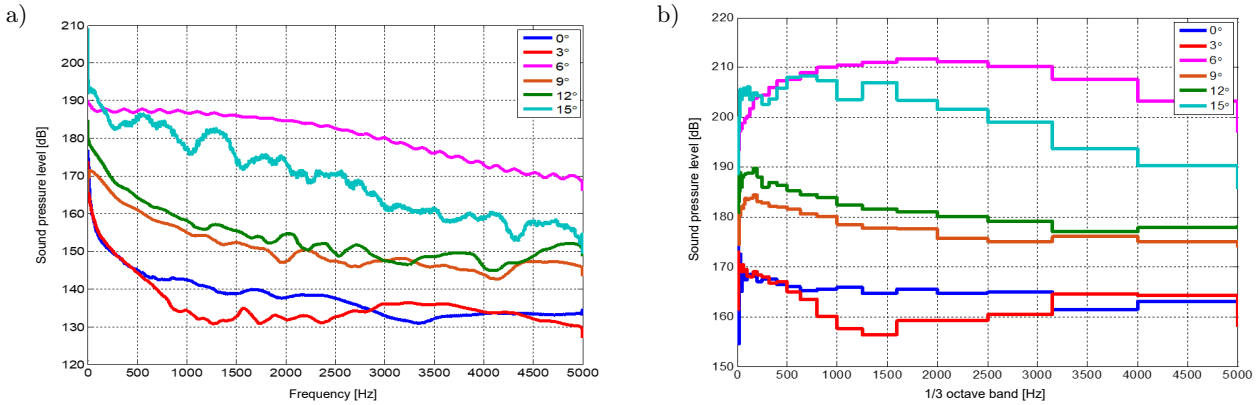

Fig. 19. Sound pressure frequency spectrum curves of R7 at 0°, 3°, 6°, 9°, 12°, 15°.

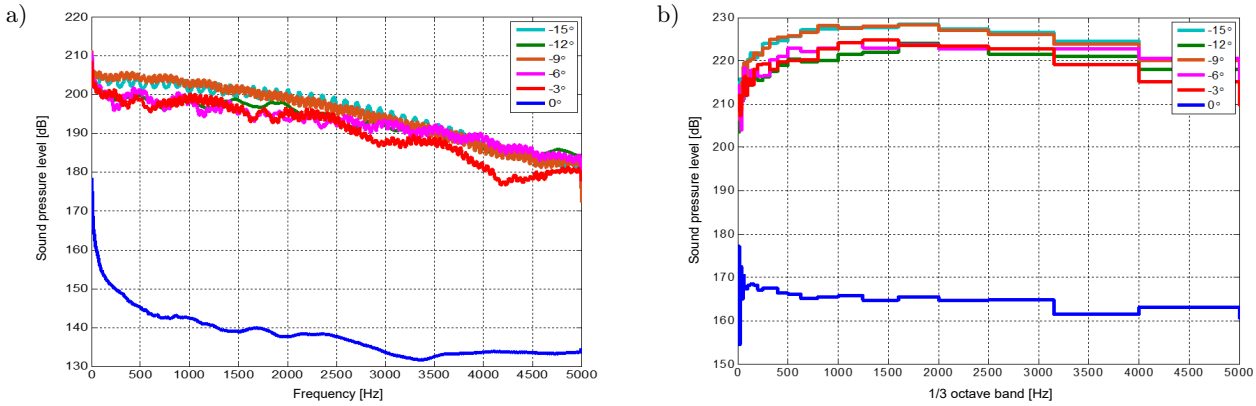

Fig. 20. Sound pressure frequency spectrum curves of R7 at 0°, −3°, −6°, −9°, −12°, −15°.

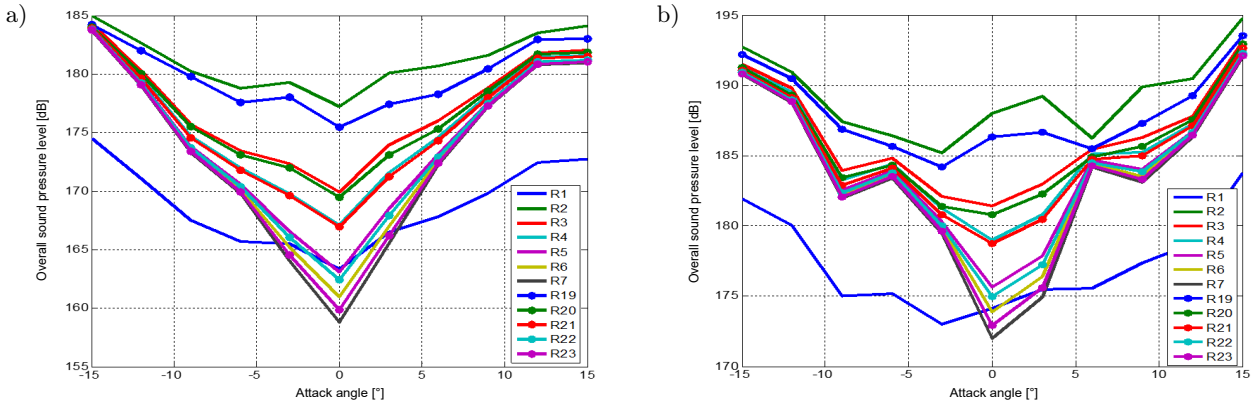

Fig. 21. The change law of overall sound pressure level with the angle at the monitoring points of the surface of the hydrofoil: a) 39.5.33 m/s; b) 10.288 m/s.

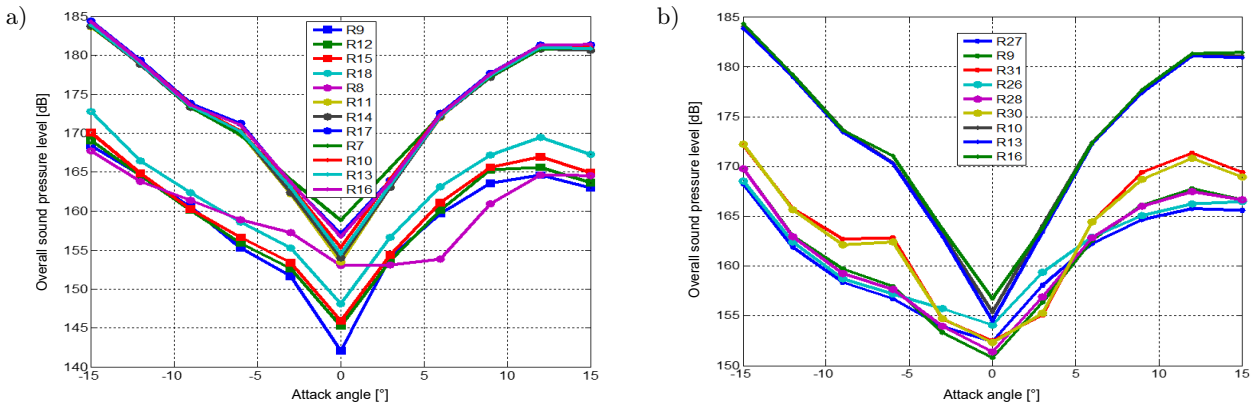

Fig. 22. The change law of overall sound pressure level with the angle at the monitoring points of the horizontal axis and below the tail of the hydrofoil (5.33 m/s).

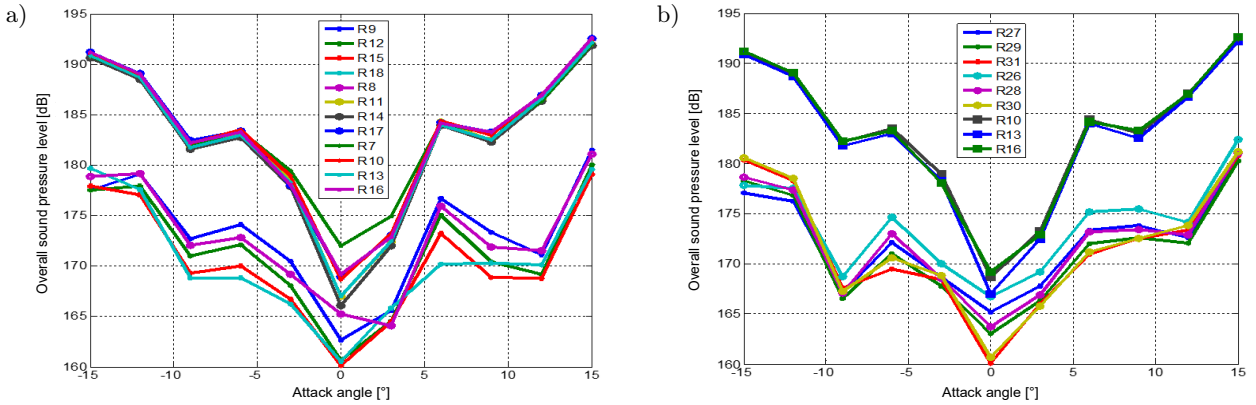

Fig. 23. The change law of overall sound pressure level with the angle at the monitoring points of the horizontal axis and below the tail of the hydrofoil (10.288 m/s).

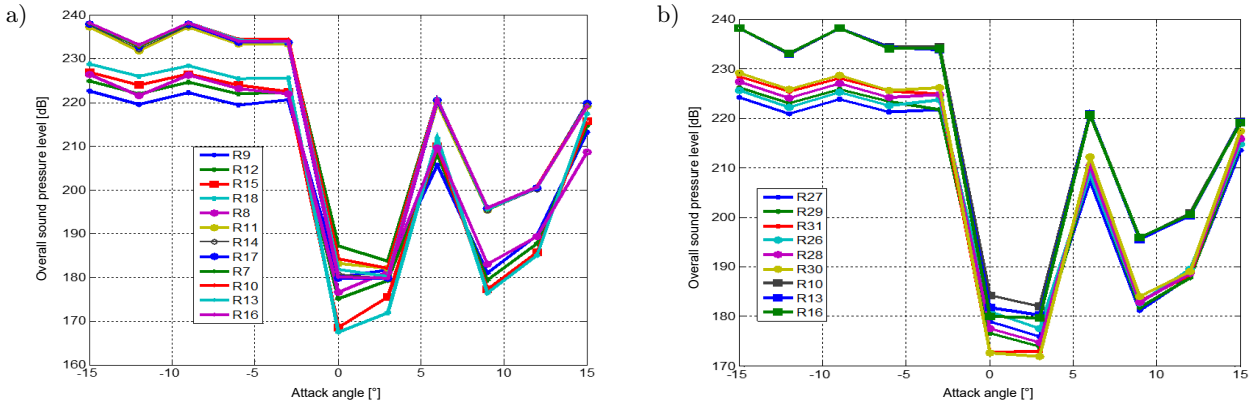

Fig. 24. The change law of overall sound pressure level with the angle at the monitoring points of the horizontal axis and below the tail of the hydrofoil (20.577 m/s).

The curve above shows that the points above the horizontal axis increase with the distance of the vertical axis, and the sound pressure level decreases gradually: SPL(R7 > R8 > R9), SPL(R10 > R11 > R12), SPL(R13 > R14 > R15), SPL(R16 > R17 > R18). At the points on the suction side of the hydrofoil, the sound pressure levels at monitoring points R2~R7 increase with the increase in the absolute value of the angle, and they reach the minimum value when the attack angle becomes 0°. The sound pressure levels at R2~R7 gradually decrease with the increase in the distance from the monitoring point at R1. The condition is the same as the pressure side.

The results in working conditions 1, 2, and 3 show that, for a specific cavitation number, the sound pressure level at each monitoring point increases with the increase in inflow velocity. In working conditions 1 and 2, the sound pressure levels at the monitoring points on the surface of the hydrofoil and the monitoring points at the tail of the hydrofoil are basically

equivalent at the positive and negative angles of attack, and 0° is the axis of symmetry. In working condition 1, the sound pressure level is attenuated by −6 dB/3° at the negative angle of attack, while at the positive angle of attack, the sound pressure level increases by 6 dB/3° at monitoring points above the horizontal axis of the tail of the hydrofoil and increases by 3 dB/3° at the points below the horizontal axis of the tail. Moreover, the sound pressure values clearly fluctuate at monitoring points R7, R9, R17, R18, R30, and R31. In working condition 2, the sound pressure level is attenuated by −6 dB/3° at the negative angle of attack, while at the positive angle, the sound pressure level increases by 4 dB/3°, at the monitoring points R7, R8, R9, and R10 of 6° to 12°, the sound pressure level is attenuated by 2.5 dB/3°. In working condition 3, with the increase in velocity, the sound pressure level at each monitoring point at the tail of the hydrofoil remains relatively consistent at negative attack angles of −15° to −3°, while there is a sharp attenuation of about 50 dB at −3° to 0°. At the positive angle of attack, the overall sound pressure level changes relatively drastically, especially at 3°~6°, and the overall sound pressure level rapidly increases by about 35 dB; however, it rapidly decreases by about 30 dB at 6°~9° and increases by about 20 dB at 12°~15°.

The computational figures of the power spectral density at monitoring points R2, R7, R18, and R31 in working condition 2 are shown in Fig. 25.

From the analysis of the power spectral density at each monitoring point at the surface or the tail of the hydrofoil, it can be observed that the power spectral densities near the surface of the hydrofoil at points R1~R6 are distinctively larger than those above at points R7~R18 for a positive attack angle and also greater than those at points R25~R31 below the horizontal axis of the hydrofoil tail. However, the power spectral densities below the horizontal axis of the hydrofoil tail are greater than those above the axis at equidistant monitoring points, which indicates that the energy near the hydrofoil surface is relatively high. With the increase in the attack angle, the power spectral density increases correspondingly.

At the negative angle of attack, the power spectral density near the surface of the hydrofoil at points R19~R23 is much higher than that at R7~R16 (above the horizontal axis of the hydrofoil tail) and greater than that at R24~R31 (below the axis of the hydrofoil

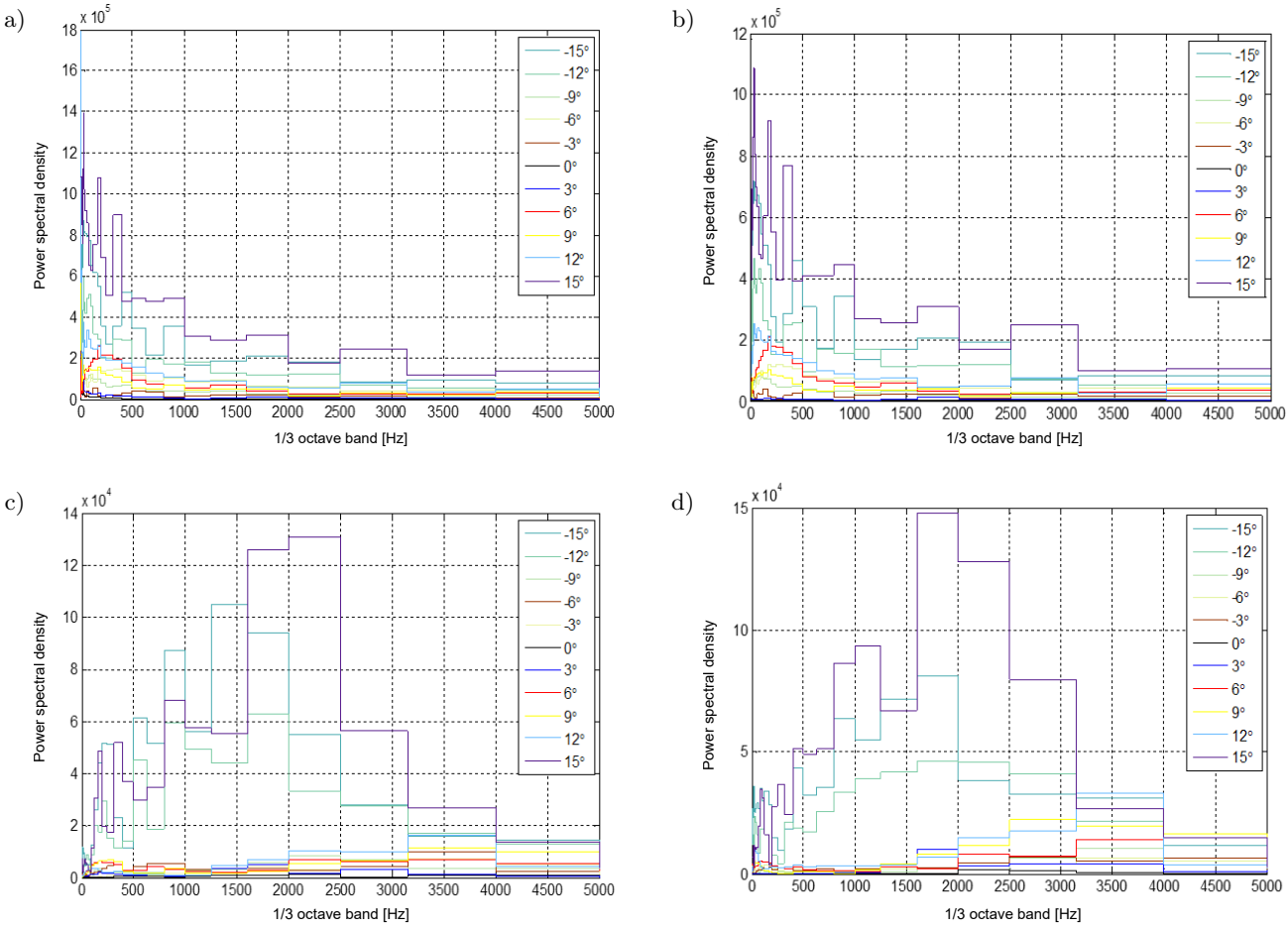

Fig. 25. Power spectral density: a) R2 point; b) R7 point; c) R17 point; d) R31 point.

tail). The power spectral density above the horizontal axis of the hydrofoil tail is greater than that below its horizontal axis at equidistant monitoring points, which indicates that the energy near the hydrofoil surface is relatively high, and the power spectral density increases with the increase in the absolute value of the attack angle.

4. Conclusions

The noise performance of a hydrofoil was numerically predicted and analyzed, and the characteristics of the sound pressure spectrum, sound power spectrum and noise changes at different monitoring points were determined. The noise characteristics and change law of the NACA66 hydrofoil with a specific cavitation number were analyzed. Cavitation bubbles experienced a periodic pulsating process of inception, development, fracture, falling-off, and bursting. With a constant cavitation number, the cavitation area of the foil becomes longer and thicker with the increase in the attack angle, and the initial position of cavitation inception moves forward. As the inflow velocity increases, changes in the cavitation noise and region become more drastic. The results in working conditions show that, for a specific cavitation number, the sound pressure level at each monitoring point increases with the increase in inflow velocity.

The change law of noise was analyzed at each monitoring point of the surface and tail of the NACA66 hydrofoil at different inflow velocities and positive and negative attack angles. The shape of cavitation bubbles has a great influence on the acoustic signal signature of the hydrofoil, particularly at the tail of the hydrofoil, and has a significant effect on the noise of the flow field at the tail. Moreover, because the monitoring points may stack, counteract or interfere with each other, the acoustic signal signatures are weakened or locally reinforced. The novelty is that the study has important calculations and analyses regarding the noise performance of a hydrofoil, characteristics of the sound pressure spectrum, and sound power spectrum and noise changes at different monitoring points. The article may be useful for specialists in the field of engineering and physics. This paper can be of interest both as introductory material and as a basis for further study.

References

1. Alkishriwi N., Meinke M., Schröder W. (2008), Large eddy simulation of steam wise-rotation turbulent channel flow, *Computer & Fluids*, **37**(7): 786–792, doi: 10.1016/j.compfluid.2007.03.018.
2. Al-Obaidi A.R. (2019), Numerical investigation of flow field behaviour and pressure fluctuations within an axial flow pump under transient flow pattern based on CFD analysis method, *Journal of Physics: Conference Series*, **1279**(1): 012069, doi: 10.1088/1742-6596/1279/1/012069.
3. Al-Obaidi A.R. (2020), Influence of guide vanes on the flow fields and performance of axial pump under unsteady flow conditions: Numerical study, *Journal of Mechanical Engineering and Sciences*, **14**(2): 6570–6593, doi: 10.15282/jmes.14.2.2020.04.0516.
4. Al-Obaidi A.R., Mishra R. (2020), Experimental investigation of the effect of air injection on performance and detection of cavitation in the centrifugal pump based on vibration technique, *Arabian Journal for Science and Engineering*, **45**(7): 5657–5671, doi: 10.1007/s13369-020-04509-3.
5. Beljatynskij A. Prentkovskis O., Krivenko J. (2010), The experimental study of shallow flows of liquid on the airport runways and automobile roads, *Transport*, **25**(4): 394–402, doi: 10.3846/transport.2010.49.
6. Cao H., Fang S., Zhu Z. (2014), Numerical prediction and characteristic analysis of slow varying components of cavitation noise of propeller in non-uniform inflow, *High-tech Communications*, **24**(3): 296–304, doi: 10.3772/j.issn.1002-0470.2014.03.012.
7. Chang F.N. (2011), The prediction of the viscous cavitation flow around a hydrofoil section, [in:] *Proceedings of the Twenty First International Offshore and Polar Engineering Conference*, **1**: 989–994, https://onepetro.org/ISOPEIOPEC/proceedings-abstract/ISOPE11/All-ISOPE11/ISOPE-I-11-423/13400 (access: 21.09.2022).
8. Curle N. (1955), The influence of solid boundaries upon aerodynamic sound, *Proceedings of the Royal Society of London, Series A*, **231**(1187): 505–514, doi: 10.1098/rspa.1955.0191.
9. Ducoin A., Astolfi J.A., Deniset F., Sigrist J.F., (2009), Computational and experimental investigation of flow over a transient pitching hydrofoil, *European Journal of Mechanics – B/Fluids*, **28**(6): 728–743, doi: 10.1016/j.euromechflu.2009.06.001.
10. Ducoin A., Astolfi J.A., Gobert M.L. (2012), An experimental study of boundary-layer induced vibrations on a hydrofoil, *Journal of Fluids and Structures*, **32**(3): 37–51, doi: 10.1016/j.jfluidstructs.2011.04.002.
11. Fan G. (2015), *Research on Vibration and Acoustic Radiation Characteristics of Hydrofoil Flow*, Shanghai, School of Mechanics and Power, Shanghai Jiao Tong University.
12. Fuji A., Kawakami D.T., Tsujimoto Y., Arndt R.E.A. (2007), Effect of hydrofoil shapes on partial and transitional cavity oscillations, *Journal of Fluids Engineering*, **129**(6): 669–673, doi: 10.1115/1.2734183.
13. Hong F., Yuan J.P., Zhou B.L. (2017), Application of a new cavitation model for computations of unsteady turbulent cavitating flows around a hydrofoil, *Journal of Mechanical Science and Technology*, **31**(1): 249–260, doi: 10.1007/s12206-016-1227-x.

14. Huang B., Wu Q., Wang G.-Y. (2018), Progress and prospects of investigation into unsteady cavitating flows [in Chinese], *Drainage and Irrigation Mechanical Engineering*, **36**(1): 1–14, doi: 10.3969/j.issn.1674-8530.17.0094.

15. Ji B., Lou X.-W., Wu Y.-L., Liu S.-H., Xu H.-Y., Oshima A. (2010), Numerical investigation of unsteady cavitating turbulent flow around a full-scale marine propeller, *Journal of Hydrodynamics*, **22**(5): 747–752, doi: 10.1016/S1001-6058(10)60025-X.

16. Kieldsen M., Arndt R.E.A., Effertz M. (2000), Spectral characteristics of sheet/cloud cavitation, *Journal of Fluids Engineering*, **122**(3): 481–487, doi: 10.1115/ 1.1287854.

17. Korzhyk V., Bushma O., Khaskin V., Dong C., Sydorets V. (2017), Analysis of the current state of the processes of hybrid laser-plasma welding, [in:] *Proceedings of the 2nd International Conference on Mechanics, Materials and Structural Engineering (ICMMSE 2017) "AER-Advances in Engineering Research"*, pp. 80–90, doi: 10.2991/icmmse-17.2017.14.

18. Kubota A., Kato H., Yamaguchi H. (1992), A new modeling of cavitating flows: a numerical study of unsteady cavitation on a hydrofoil section, *Journal of Fluid Mechanics*, **240**(1): 59–96, doi: 10.1017/S00221 1209200003X.

19. Leroux J.B., Astolfi J.A., Billard J.Y. (2004), An experimental study of unsteady partial cavitation, *Journal of Fluids Engineering*, **126**(1): 94–101, doi: 10.1115/1.1627835.

20. Leroux J.B., Olivier C.D., Astolfi J.A. (2003), A joint experimental and numerical study of mechanisms associated to instability of partial cavitation on two-dimensional hydrofoil, *Physics of Fluids*, **17**(5): 052101, doi: 10.1063/1.1865692.

21. Li G., Shi L. (1997), Cavitation and cavitation erosion and their influencing factors [in Chinese], *Journal of Petroleum University (Natural Science Edition)*, **21**(1): 97–101, http://www.alljournals.cn/view_abstract.aspx?pcid=3C5CA5E51F7D0F8A&cid=3C5CA5E51F7D0F8A&jid=AFEA5AA653DB650F7CB44EE42E99DE56&aid=4D3C8AFBB3796195B9EA80098C763CE8&yid=5370399DC954B911&vid=&iid=&sid=&eid=&from_absract=1 (access: 11.09.2022).

22. Lord Rayleigh O.M. F.R.S. (1917), VIII. On the pressure developed in a liquid during the collapse of a spherical cavity, *The London, Edinburgh, and Dublin Philosophical Magazine and Journal of Science*, **34**(200): 94–98, doi: 10.1080/14786440808635681.

23. Neppiras E.A., Noltingk B.E. (1951), Cavitation produced by ultrasonics: Theoretical conditions for the onset of cavitation, *Proceedings of The Physical Science Society, Section B*, **64**(12): 1032–1038, doi: 10.1088/0370-1301/64/12/302.

24. Noltingk B.E., Neppiras E.A. (1950), Cavitation produced by ultrasonics, *Proceedings of the Physical Society, Section B*, **63**(9): 674–685, doi: 10.1088/0370-1301/63/9/305.

25. Nurtas M., Baishemirov Z., Tsay V., Tastanov M., Zhanabekov Z. (2020), Convolutional neural networks as a method to solve estimation problem of acoustic wave propagation in poroelastic media, *News of the National Academy of Sciences of the Republic of Kazakhstan – Physico-Mathematical Series*, **4**(332): 52–60, doi: 10.32014/2020.2518-1726.65.

26. Plesset M. (1949), The dynamics of cavitation bubbles, *Journal of Applied Mechanics*, **16**: 277–282.

27. Prentkovskis O., Tretjakovas J., Švedas A., Bieliatynskyi A., Daniūnas A., Krayushkina K. (2012), The analysis of the deformation state of the double-wave guardrail mounted on bridges and viaducts of the motor roads in Lithuania and Ukraine, *Journal of Civil Engineering and Management*, **18**(5): 761–771, doi: 10.3846/13923730.2012.731252.

28. Prokopov V.G. *et al.* (1993), Effect of coating porosity on the process of heat-transfer with gas-thermal deposition, *Powder Metallurgy and Metal Ceramics*, **32**(2): 118–121, doi: 10.1007/BF00560034.

29. Schnerr G.H., Sauer J. (2001), Physical and numerical modeling of unsteady cavitation dynamics, [in:] *4th International Conference on Multiphase Flow ICMF-2001*, https://www.semanticscholar.org/paper/Physical-and-numerical-modeling-of-unsteady-Schnerr-Sauer/ed8c0ec44ddc18456eb4f32fb7aaf76605bd13aa (access: 17.09.2022).

30. Shin S., Hong J.-W., Nagarathinam D., Ahn B.-K., Park S.-G. (2021), Tip vortex cavitation and induced noise characteristics of hydrofoils, *Applied Sciences (Switzerland)*, **11**(13): 5906, doi: 10.3390/app11135906.

31. Singhal A.K., Athavale M.M., Li H., Jiang Y. (2002), Mathematical basis and validation of the full cavitation model, *Journal of Fluids Engineering*, **124**(3): 617–624, doi: 10.1115/1.1486223.

32. Su Y., Dou F., Liu Y., Cui T. (2013), Study of non-cavitating propeller noise, *Journal of Wuhan University of Technology (Transportation Science and Engineering)*, **37**(5): 895–899, doi: 10.3963/j.issn.2095-3844.2013.05.001.

33. Sultanov K.S., Khusanov B.E., Rikhsieva B.B. (2020), Longitudinal waves in a cylinder with active external friction in a limited area, [in:] *IV International Scientific and Technical Conference Mechanical Science and Technology Update (MSTU-2020)*, **1546**: 012140, doi: 10.1088/1742-6596/1546/1/012140.

34. Wang G., Senocak I., Shyy W., Ikohagi T., Cao S. (2001), Dynamics of attached turbulent cavitating flow, *Progress in Aerospace Science*, **37**(6): 551–581, doi: 10.1016/S0376-0421(01)00014-8.

35. Wang G., Ostoja-Starzewski M. (2007), Large eddy simulation of a sheet/cloud cavitation on a NACA0015 hydrofoil, *Applied Mathematical Modelling*, **31**(3): 417–447, doi: 10.1016/j.apm.2005.11.019.

36. Wang G.-Y., Zhang B., Huang B., Zhang M. (2009), Unsteady dynamics of cloud cavitating flows around

a hydrofoil, *Journal of Experiments in Fluid Mechanics*, **23**(3): 44–49, https://www.semanticscholar.org/paper/Unsteady-Dynamics-of-Cloud-Cavitating-Flows-around-Wang-Zhang/0db160f3faecc68c656b97b6453252fba40eeded (access: 19.09.2022).

37. Wang W., Li Z., Liu M., Ji X. (2021), Influence of water injection on broadband noise and hydrodynamic performance for a NACA66 (MOD) hydrofoil under cloud cavitation condition, *Applied Ocean Research*, **115**: 102858, doi: 10.1016/j.apor.2021.102858.
38. Wu J.Y., Wang G.Y., Shyy W. (2005), Time-dependent turbulent cavitating flow computations with interfacial transport and filter based models, *International Journal for Numerical Methods in Fluids*, **49**(7): 739–761, doi: 10.1002/fld.1047.
39. Yang Q., Wang Y., Zhang Z. (2012), Assessment of the improved cavitation model and modified turbulence model for ship propeller cavitation simulation, *Journal of Mechanical Engineering*, **48**(9): 178–785, doi: 10.3901/JME.2012.09.178.
40. Yang Q., Wang Y., Zhang Z., Hou G. (2014), Numerical prediction of cavitation inception radiated noise of contra-rotating propeller with non-uniform in flow, *Shenghxue Xuebao/Acta Acustica*, **39**(5): 589–604.
41. Yang Q.-F., Wang Y.-S., Zhang Z.-H. (2011), Improvement and evaluation of numerical model for cavitation flow viscous simulation around propeller blade section, *Transactions of Beijing Institute of Technology*, **31**(12): 1401–1407.
42. Zhang B., Wang G., Huang B., Zhiyi Y. (2009), Numerical and experimental studies on unsteady shedding mechanisms of cloud cavitation, *Chinese Journal of Theoretical and Applied Mechanics*, **41**(5): 651–659, doi: 10.6052/0459-1879-2009-5-2008-152.
43. Zwart P., Gerber A.G., Belamri T. (2004), A two-phase flow model for prediction cavitation dynamics, [in:] *5th ICMF 2004 International Conference on Multiphase Flow*.